Biogeosciences Discuss., 10, 14475–14514, 2013
www.biogeosciences-discuss.net/10/14475/2013/
doi:10.5194/bgd-10-14475-2013

Biogeosciences Discussions
Open Access

Influence of river discharge on phytoplankton absorption properties: a case study in the East China Sea and Tsushima Strait

S. Wang[1], J. Ishizaka[2], H. Yamaguchi[3], S. C. Tripathy[4], M. Hayashi[1], Y. Xu[1], Y. Mino[2], T. Matsuno[5], Y. Watanabe[6], and S. Yoo[7]

[1]Graduate School of Environmental Studies, Nagoya University, Nagoya, Japan
[2]Hydrospheric Atmospheric Research Center, Nagoya University, Nagoya, Japan
[3]Earth Observation Research Center, Japan Aerospace Exploration Agency, Tsukuba, Japan
[4]National Centre for Antarctic and Ocean Research, Goa, India
[5]Research Institute for Applied Mechanics, Kyushu University, Kasuga, Japan
[6]The General Environmental Technos Co., LTD, Osaka, Japan
[7]Korea Institute of Ocean Science and Technology, Ansan, Korea

Received: 15 August 2013 – Accepted: 19 August 2013 – Published: 29 August 2013

Correspondence to: S. Wang (wang.shengqiang@e.mbox.nagoya-u.ac.jp)

Published by Copernicus Publications on behalf of the European Geosciences Union.

Abstract

To investigate the influence of fresh water on phytoplankton absorption properties, the phytoplankton absorption coefficient and pigments identified by high-performance liquid chromatography (HPLC) were measured at the surface and subsurface chlorophyll *a* maximum (SCM) in the East China Sea (ECS), which is highly influenced by river discharge from the Changjiang during summer. For comparison, data were also collected in the Tsushima Strait (TS) at the surface and SCM. The majority of ECS surface samples taken from the low-salinity Changjiang diluted water (CDW), and even most of SCM samples taken from waters beneath the CDW, displayed significant freshwater influences. The specific absorption coefficient normalized by total chlorophyll *a* concentration (Tchl *a*), $a^*_{ph}(\lambda)$, of these samples was substantially higher than values derived from global regressions between $a^*_{ph}(\lambda)$ and the Tchl *a*. Using the pigment data derived from HPLC, the increase of $a^*_{ph}(\lambda)$ was found to be mainly caused by the phytoplankton size structure, which indicated that both surface and SCM samples in the ECS still incorporated considerable portions of picophytoplankton (cyanobacteria), even though the Tchl *a* was high. When water from the surface and the SCM were merged, variations in the phytoplankton size-fractions and $a^*_{ph}(\lambda)$ vs. Tchl *a* that were consistent with values for the global ocean were found in the TS but not in the ECS. Data for the ECS indicated that there was no correlation between Tchl *a* and the size-fraction or total pigment absorption. As a consequence, $a^*_{ph}(\lambda)$ was poorly correlated with Tchl *a* and displayed large variability within a small Tchl *a* range. These findings suggest the need for care when considering the changing patterns of size-fractions vs. Tchl *a* and the relationship between $a^*_{ph}(\lambda)$ and Tchl *a* in coastal regions that are significantly influenced by fresh water.

BGD
10, 14475–14514, 2013

1 Introduction

Phytoplankton light absorption is a major factor in determining the optical properties of oceanic and coastal waters. The process has the potential to change the underwater light fields, modulate photosynthesis, and alter the ocean colour (Gordon et al., 1988; Morel, 1988). Knowledge of phytoplankton light absorption and its variation is vital for understanding the optical variability of water bodies, and therefore improving a variety of bio-optical algorithms, such as for remote sensing of chlorophyll *a* concentration (Chl *a*) (Garver and Siegel, 1997; He et al., 2000), primary production (Platt and Sathyendranath, 1988; Ishizaka, 1998), and phytoplankton size classes (Ciotti and Bricaud, 2006; Hirata et al., 2008; Devred et al., 2011).

In recent decades, phytoplankton light absorption has been extensively investigated in various regions of the world. It is well documented that the phytoplankton absorption coefficient, $a_{ph}(\lambda)$, is positively correlated with Chl *a* and that this correlation holds fairly well for various water bodies (Cleveland, 1995; Babin et al., 2003; Bricaud et al., 2004). The Chl *a*-specific absorption coefficient, $a^*_{ph}(\lambda)$, is defined as the ratio of $a_{ph}(\lambda)$ to Chl *a*, and its temporal/spatial variations have been reported for various water bodies (Babin et al., 1993; Bricaud et al., 1995; Suzuki et al., 1998; Harimoto et al., 1999; Stæhr et al., 2004). The general tendency is that $a^*_{ph}(\lambda)$ decreases with an increase in Chl *a*, and Bricaud et al. (1995) found that both horizontal and vertical covariations of $a^*_{ph}(\lambda)$ and Chl *a* followed similar trends. The packaging effect and pigment composition are suggested to be the major factors causing the variability in $a^*_{ph}(\lambda)$ (Morel and Bricaud, 1981; Stuart et al., 1998; Lohrenz et al., 2003). These two factors are different among and within phytoplankton populations growing under various environmental conditions (e.g., nutrient levels, irradiance).

Large phytoplankton generates a strong packaging effect, producing low $a^*_{ph}(\lambda)$, while the packaging effect of small phytoplankton is less and results in high $a^*_{ph}(\lambda)$. Changes in the phytoplankton size structure have been reported to explain variations in $a^*_{ph}(\lambda)$ (Ciotti et al., 2002; Bricaud et al., 2004). Sathyendranath et al. (2001) expressed $a_{ph}(\lambda)$

BGD
10, 14475–14514, 2013

as the sum of absorption by two populations with a distinct cell size, and this model was further extended to a three population model by Brewin et al. (2011). More recently, absorption models based on two or three population sizes have been improved to estimate the $a^*_{ph}(\lambda)$ of different populations as well as to derive phytoplankton size-fractions from the $a_{ph}(\lambda)$ (Devred et al., 2006, 2011). Note that these models are based on the hypothesis that small and large cells dominate in low and high Chl *a* waters, respectively, which has been clearly observed in the global ocean (Brewin et al., 2010; Hirata et al., 2011).

However, in coastal waters it is not known whether this hypothesis is valid. Because of the dynamic hydrographic conditions in coastal regions (e.g., discharge, upwelling, and mixing), the optical properties of water are complex (Babin et al., 2003). Some studies have shown that freshwater discharges could significantly change the optical properties of seawater, especially the light absorption budget among phytoplankton, detritus, and colored dissolved organic matter (Babin et al., 2003; Matsuoka et al., 2011; Brunelle et al., 2012). However, freshwater effects, specifically on the phytoplankton absorption properties, such as the variability in $a^*_{ph}(\lambda)$ and the correlations between Chl *a* with $a_{ph}(\lambda)$ and $a^*_{ph}(\lambda)$, have not been well examined.

The East China Sea (ECS), the largest marginal sea in the western North Pacific, is significantly influenced by river discharge from the Changjiang (Gong et al., 1996). In summer, the ECS receives enormous amounts of fresh water containing very high concentrations of nitrogen (Gong et al., 1996; Siswanto et al., 2008). The nutrient-rich fresh water mixes with the surrounding high-salinity waters forming Changjiang diluted water (CDW), which extends offshore and moves north-eastward near Jeju Island to the Tsushima Strait (TS) (Yamaguchi et al., 2012). It has been suggested that the CDW enhances Chl *a*, resulting in high primary production in the upper layer of the ECS (Hama et al., 1997; Yamaguchi et al., 2012). The phytoplankton community has also been reported to be modulated by Changjiang fresh water in the estuary and adjacent coastal waters (Zhou et al., 2008). Therefore, Changjiang fresh water is likely

BGD
10, 14475–14514, 2013

to have an influence on phytoplankton light absorption in the ECS, especially in the surface layer.

The TS, which is a narrow and shallow strait between Korea and Japan, connects the ECS and the Sea of Japan. Water in the TS originates partly from the Kuroshio but mainly from the ECS in summer (Guo et al., 2006). Fresh water and nutrients are transported from the ECS through the TS to the Sea of Japan (Isobe et al., 2002; Morimoto et al., 2009). Yamaguchi et al. (2012) observed that about two months was required for the CDW to reach the TS, where the enhancement in surface Chl *a* was very small with a slight peak in September. Morimoto et al. (2009) suggested that when the CDW extended into the TS, nutrients were consumed by phytoplankton and depleted. These studies imply that the influence of Changjiang fresh water on phytoplankton in the TS may be weak.

In this study, considering the strong influence of Changjiang fresh water on the ECS in summer, we hypothesize that the phytoplankton absorption properties in the ECS may be different from those in the TS. The objective of this study was to test this hypothesis on the basis of phytoplankton light absorption and pigment data derived from high-performance liquid chromatography (HPLC). For this purpose, (1) differences in the phytoplankton light absorption between the ECS and TS were characterized at both the surface and subsurface Chl *a* maximum (SCM). The vertical variations in phytoplankton absorption (differences between the surface and SCM) were also compared between the ECS and TS. (2) Correlations between total Chl *a* (Tchl *a*) with $a_{ph}(\lambda)$ and $a^*_{ph}(\lambda)$ in all samples from the surface and SCM were investigated in both the ECS and TS. To completely understand these differences in phytoplankton light absorption between the ECS and TS, the size structure derived from HPLC pigment data, the packaging effect, and pigment composition were studied.

BGD
10, 14475–14514, 2013

2 Materials and methods

2.1 Sampling

Sampling in the TS was conducted during a cruise in July 2008 aboard the T/V *Nagasaki maru*. Four cruises were conducted in the ECS in August 2008 and July 2009–2011 aboard the R/V *Tansei maru* and the T/V *Nagasaki maru*, respectively (Table 1). The locations of sampling stations are shown in Fig. 1. Water samples at discrete depths were collected using Niskin bottles (12 L on the R/V *Tansei maru*; 5 L on the T/V *Nagasaki maru*) mounted on a CTD/rosette system. According to the fluorescence profile, the sampling depth of the SCM was determined from its prominent biological features. Samples collected at the surface and SCM were used to measure $a_{ph}(\lambda)$ and pigment concentrations.

2.2 Measurement of absorption coefficient

The quantitative filter technique (QFT) was used to determine $a_{ph}(\lambda)$ (Mitchell, 1990). Water samples were filtered through Whatman GF/F glass fibre filters (25 mm) under low vacuum pressure (< 0.01 MPa). Subsequently, the optical density of particles retained on the filter ($OD_f(\lambda)$) was measured between 350 and 750 nm at 1 nm intervals, using a dual beam multi-purpose spectrophotometer (MPS-2400, Shimadzu Inc.). A blank filter soaked with 0.2-µm-filtered seawater (FSW) was used as the reference. The $OD_f(750)$ was subtracted from all wavelengths to minimize the difference between the sample and reference filter, assuming no absorption at 750 nm. To correct for the path length amplification effect caused by multiple scattering in the glass-fibre filter, the following equation was utilized according to Cleveland and Weidemann (1993):

$$OD_s(\lambda) = 0.378OD_f(\lambda) + 0.523OD_f(\lambda)^2 \quad (1)$$

BGD
10, 14475–14514, 2013

where $OD_s(\lambda)$ is the optical density of particulate matter in suspension. The absorption coefficient of the particulate matter ($a_p(\lambda)$) was calculated using the following equation:

$$a_p(\lambda) = 2.303 OD_s(\lambda) S/V \quad (2)$$

where 2.303 is the factor used to convert $\log_{10}$ to $\log_e$, S is the filter clearance area (m^2), and V is the filtered volume (m^3). The ratio of S to V stands for the geometrical light pass length.

After measurements of the optical density of the particulate matter, the filters were soaked in methanol for at least 24 h to extract phytoplankton pigments, and then rinsed with FSW. The absorbance of a decolorized filter was re-measured using the same method to obtain the optical density of the non-phytoplankton particles (Kishino et al., 1985). Similarly, the absorption coefficient of non-phytoplankton particles ($a_d(\lambda)$) was determined using Eqs. (1) and (2). The $a_{ph}(\lambda)$ was then obtained from the following equation:

$$a_{ph}(\lambda) = a_p(\lambda) - a_d(\lambda) \quad (3)$$

The reported values in this study are averages from duplicated measurements. The $a^*_{ph}(\lambda)$ was calculated by standardizing $a_{ph}(\lambda)$ by the Tchl *a* measured by HPLC. Tchl *a* refers to the sum of Chl *a*, chlorophyllide a, and divinyl Chl *a*.

2.3 Pigment measurements and pigment-based size structure

Water samples used for the measurement of pigment concentrations were filtered onto 25 mm Whatman GF/F glass fibre filters under low vacuum pressure (< 0.01 MPa). The filtered volumes of most of samples were 1 L. The filters were immediately frozen in liquid nitrogen, and were then stored in a −80 °C freezer on shore for later laboratory analysis. Pigments were analyzed by reverse-phase HPLC with a Zorbax Eclipse XDB-C8 column (150 mm × 4.6 mm, 3.5 µm; Agilent Technologies), and 19 pigments were separated and quantified following the method of Van Heukelem and Thomas (2001).

BGD
10, 14475–14514, 2013

Diagnostic pigment analysis (DPA) was then used to estimate the Tchl *a* fractions of pico- (< 2 µm), nano- (2–20 µm) and micro-phytoplankton (> 20 µm), from HPLC pigment data. The DPA approach was originally proposed by Vidussi et al. (2001), and refined by Uitz et al. (2006). Briefly, seven marker pigments (MP) (i.e., fucoxanthin (Fuco), peridinin (Per), 19′-hexanoyloxyfucoxanthin (Hex), 19′-butanoyloxyfucoxanthin (But), alloxanthin (Allo), chlorophyll *b* (Chl *b*), and zeaxanthin (Zea)) were selected as being representative of distinct phytoplankton groups and were used to calculate the Tchl *a* fractions of three size classes (detailed pigment taxonomic significance reported previously by Vidussi et al., 2001 and Uitz et al., 2006). Subsequently, Hirata et al. (2008) further revised the approach of Uitz et al. (2006) to account for the occurrence of Chl *b* in larger eukaryotes, e.g., chlorophytes (nano-phytoplankton). According to Hirata et al. (2008), the size-fractions of each size class can be expressed as

$$f_{\text{micro}} = (1.41\,\text{Fuco} + 1.41\,\text{Per})/\text{DP} \quad (4)$$

$$f_{\text{nano}} = (0.60\,\text{Allo} + 0.35\,\text{But} + 1.27\,\text{Hex} + 1.01\,\text{Chl}\,b)/\text{DP} \quad (5)$$

$$f_{\text{pico}} = 0.86\,\text{Zea}/\text{DP} \quad (6)$$

where DP is the sum of the weighted concentrations of all diagnostic pigments:

$$\text{DP} = 1.41\,\text{Fuco} + 1.41\,\text{Per} + 0.60\,\text{Allo} + 0.35\,\text{But} + 1.27\,\text{Hex} + 1.01\,\text{Chl}\,b + 0.86\,\text{Zea} \quad (7)$$

The numerical coefficients used in the above equations, which were derived by multiple regressions (Uitz et al., 2006), represent the ratios of Tchl *a* to each diagnostic pigment. Hirata et al. (2008) suggested that a particular phytoplankton size class was dominant if its fraction was greater than 0.45. It should be noted that there are some potential anomalies in DPA, e.g., in some cases, a given diagnostic pigment possibly occurs in two size classes. Despite these potential limitations, DPA is a useful approximation, and the results are reasonably robust at a global as well as at a regional scale.

BGD
10, 14475–14514, 2013

2.4 Packaging effect index and total pigment absorption

The packaging effect index, $Q_a^*(\lambda)$, is defined as the ratio of the in vivo absorption coefficient ($a_{ph}(\lambda)$) to the absorption coefficient of the same cellular material in solvent condition ($a_{sol}(\lambda)$) (Bricaud et al., 2004). The computation is expressed as follows:

$$Q_a^*(\lambda) = a_{ph}(\lambda)/a_{sol}(\lambda) \quad (8)$$

The theoretical maximum and minimum values of $Q_a^*(\lambda)$ are 1 and 0, corresponding to conditions without a packaging effect and with the maximal packaging effect, respectively. Bricaud et al. (2004) stated that the $a_{sol}(\lambda)$ reconstructed from all individual pigments was systematically lower than the measured $a_{ph}(\lambda)$ and argued that differences between measured and reconstructed absorption spectra could be attributed to missing pigments or other light-absorbing compounds extracted by methanol but not measured by HPLC. Considering the missing absorption term, $a_{sol}(\lambda)$ is calculated as

$$a_{sol}(\lambda) = \sum C_i a^*_{pigm,i}(\lambda) + a_{miss}(\lambda) \quad (9)$$

where C_i and $a^*_{pigm,i}(\lambda)$ are the concentration and the pigment-specific absorption coefficient of the ith pigment, respectively, and $a_{miss}(\lambda)$ is the missing absorption. In this study, $a_{miss}(440)$ was estimated according to Bricaud et al. (2004), and then $Q_a^*(440)$ was calculated.

The total pigment-specific absorption coefficient is defined as the Tchl *a* normalized absorption coefficient of all the pigments (Bricaud et al., 2004), as in Eq. (10):

$$a^*_{pigm}(\lambda) = \sum C_i a^*_{pigm,i}(\lambda)/\text{Tchl } a \quad (10)$$

Linear regression analysis was performed to assess the relative contribution to the variation in $a^*_{ph}(\lambda)$ from the packaging effect and pigment composition, taking $a^*_{ph}(\lambda)$ as the dependent variable and $Q_a^*(\lambda)$ or $a^*_{pigm}(\lambda)$ as the independent variable. Note that the

BGD
10, 14475–14514, 2013

approach used to obtain $a^*_{pigm}(\lambda)$ was completely independent of $a^*_{ph}(\lambda)$, whereas the approach used for $Q^*_a(\lambda)$ depended on $a^*_{ph}(\lambda)$. In addition, the analyses performed in this study mainly focused on the 440 nm region because the effects of both pigment packaging and composition are more pronounced in the blue region (Stuart et al., 1998).

3 Results

3.1 Variations in Tchl *a*

Tchl *a* in water from the Tsushima Strait surface (TS_S), the Tsushima Strait SCM (TS_SCM), the East China Sea surface (ECS_S), and the East China Sea SCM (ECS_SCM) displayed clear differences (Table 2). The average Tchl *a* in the TS_S was lower than that in the ECS_S, and the average Tchl *a* in the TS_SCM was also lower than in the ECS_SCM. The difference between the average Tchl *a* values in the ECS_S and the ECS_SCM was larger than the difference between the corresponding values in the TS_S and TS_SCM. The coefficient of variation of Tchl *a* was similar among the TS_SCM, ECS_S, and ECS_SCM, and was lowest for the TS_S.

3.2 Variations of absorption coefficient

The average $a_{ph}(\lambda)$ values in the TS_S, TS_SCM, ECS_S, and ECS_SCM clearly differed (Fig. 2a and Table 2). The average $a_{ph}(\lambda)$ was lowest in the TS_S and much higher in the ECS_S. The average $a_{ph}(\lambda)$ in the TS_SCM was also much lower than in the ECS_SCM. The difference in average $a_{ph}(\lambda)$ between the surface and SCM was larger in the ECS than in the TS. The coefficients of variation of $a_{ph}(440)$ and $a_{ph}(675)$ of the ECS_S were the highest with values of 69.7 % and 73.7 %, respectively, and those of TS_S were the lowest with values of 27.9 % and 25.2 %, respectively. However, the coefficients of variation of $a_{ph}(440)$ and $a_{ph}(675)$ were similar for the TS_SCM

BGD
10, 14475–14514, 2013

and ECS_SCM. The different characteristics of $a_{ph}(\lambda)$ in each area generally corresponded to the variations in Tchl *a*.

As in previous studies (Bricaud et al., 1995, 2004), the $a_{ph}(440)$ and $a_{ph}(675)$ were positively correlated with the Tchl *a* in the TS and ECS (Fig. 3a and b). Here, $a_{ph}(\lambda)$ in the surface and SCM waters were combined for analysis. The fitted power law functions were as follows. For the TS,

$$a_{ph}(440) = 0.0436\,\text{Tchl}\,a^{0.626}, \quad (R^2 = 0.871,\ N = 25) \tag{11}$$

$$a_{ph}(675) = 0.0192\,\text{Tchl}\,a^{0.852}, \quad (R^2 = 0.930,\ N = 25) \tag{12}$$

and for the ECS,

$$a_{ph}(440) = 0.0667\,\text{Tchl}\,a^{0.885}, \quad (R^2 = 0.861,\ N = 118) \tag{13}$$

$$a_{ph}(675) = 0.0252\,\text{Tchl}\,a^{1.007}, \quad (R^2 = 0.898,\ N = 118) \tag{14}$$

where R^2 and N are the determination coefficients and the number of samples, respectively. The power law functions for the TS agreed well with those given by Bricaud et al. (1995), whereas most of the ECS samples significantly diverged from the regressions of Bricaud et al. (1995) (Kolmogorov-Smirnov test, $P < 0.01$), especially at high Tchl *a*. In comparison to $a_{ph}(675)$, $a_{ph}(440)$ was more scattered, with the differences caused by the absorption of accessory pigments as discussed later (Bricaud et al., 1995; Stuart et al., 1998).

3.3 Variations of Tchl *a*-specific absorption coefficient

Large variations were observed among values of the $a^*_{ph}(\lambda)$ from all the samples (Table 2). The $a^*_{ph}(440)$ and $a^*_{ph}(675)$ ranged from 0.017 to 0.158 $m^2\,mg^{-1}$ (average and standard deviation of $0.068 \pm 0.023\,m^2\,mg^{-1}$) and from 0.008 to 0.055 $m^2\,mg^{-1}$ (average and standard deviation of $0.026 \pm 0.007\,m^2\,mg^{-1}$), respectively. The coefficients of

BGD
10, 14475–14514, 2013

variation of $a^*_{ph}(440)$ and $a^*_{ph}(675)$ were 34.0 % and 29.0 %, respectively. The ratio of $a^*_{ph}(440)/a^*_{ph}(675)$ was 2.68 ± 0.56 (range: 1.80–4.60). These variations in $a^*_{ph}(\lambda)$ were consistent with results reported in previous studies (Bricaud et al., 1995; Harimoto et al., 1999).

The average $a^*_{ph}(\lambda)$ in the TS_S, TS_SCM, ECS_S, and ECS_SCM displayed distinct differences in both their magnitude and spectrum shape (Fig. 2c and Table 2). The largest differences were observed in the magnitude of absorption in the blue wavelength. The highest average $a^*_{ph}(\lambda)$ in the blue region was observed in the TS_S, and the lowest average $a^*_{ph}(\lambda)$ at most wavelengths and the flattest spectral shape was observed in the TS_SCM. The average $a^*_{ph}(\lambda)$ in the ECS_S and ECS_SCM lay between the average values in the TS_S and TS_SCM, and the average $a^*_{ph}(\lambda)$ in the ECS_S was higher than the value in the ECS_SCM. The standard deviation of $a^*_{ph}(440)$ indicated high variances in the TS_S and ECS_S, lower variances in the ECS_SCM, and the lowest variance in the TS_SCM. In addition, the $a^*_{ph}(\lambda)$ in the TS_S and ECS_S had distinct peaks around 490 nm, probably owing to the presence of the photoprotective pigment zeaxanthin (Barlow et al., 2002). A significant positive correlation between $a_{ph}(490)$ and the zeaxanthin concentration ($P < 0.01$, $R^2 = 0.751$) was observed in those samples (data not shown). The $a^*_{ph}(\lambda)$ of most samples from the ECS_SCM exhibited a clear peak around 540 nm, which possibly resulted from the absorption of phycoerythrin (Hoge et al., 1999; Ciotti et al., 2002).

The variations in $a^*_{ph}(440)$ and $a^*_{ph}(675)$ were different between the TS and ECS. Negative power correlations of Tchl *a* with $a^*_{ph}(440)$ ($P < 0.01$, $R^2 = 0.708$) (Fig. 3c) and with $a^*_{ph}(675)$ ($P < 0.01$, $R^2 = 0.287$) were recorded in the TS (Fig. 3d). The fitted power law functions for the TS were close to those obtained by Bricaud et al. (1995) in the global ocean. However, in the ECS, the power correlation between $a^*_{ph}(440)$ and Tchl *a* was poor ($P < 0.01$, $R^2 = 0.094$) and there was also no significant power correlation between $a^*_{ph}(675)$ and Tchl *a* ($P = 0.84$, $R^2 = 0.000$).

BGD
10, 14475–14514, 2013

The salinity clearly differed between the TS_S and ECS_S (Fig. 3). The salinity in TS_S was higher than 32 (average of 32.5). However, the salinity of most of the ECS_S samples (60 out of 67) was lower than 32 (average of 29.9). All the TS_SCM samples were taken from waters beneath the TS_S high-salinity water. Most of the ECS_SCM samples (45 out of 51) were collected beneath the ECS_S low-salinity water. Even at the SCM, the local salinity was also lower in the ECS than in the TS, with average values of 31.8 and 34.0, respectively (data not shown). From Fig. 3c and d, it was also found that the $a^*_{ph}(440)$ and $a^*_{ph}(675)$ of high salinity water samples from the TS and ECS were clustered around the regression lines of Bricaud et al. (1995). However, most of samples from the ECS_S low salinity water (< 32) and the corresponding ECS_SCM samples taken from waters beneath them displayed higher $a^*_{ph}(440)$ and $a^*_{ph}(675)$ comparing with values from the regressions of Bricaud et al. (1995).

3.4 Variations in the packaging effect

The $Q^*_a(440)$ showed very similar variations to those observed for the $a^*_{ph}(440)$ (Fig. 4a). The determination coefficients (R^2) of a linear regression between $a^*_{ph}(440)$ and $Q^*_a(440)$ were 0.869, 0.978, and 0.843 for all locations, the TS, and the ECS, respectively. In general, the average $Q^*_a(440)$ in the TS_S, TS_SCM, ECS_S, and ECS_SCM were consistent with the average $a^*_{ph}(440)$ in these regions. The highest and lowest average $Q^*_a(440)$, with values of 0.72 ± 0.17 and 0.40 ± 0.11, were recorded in the TS_S and TS_SCM, respectively, and the average $Q^*_a(440)$ in the ECS_S and ECS_SCM were 0.64 ± 0.19 and 0.61 ± 0.16, respectively.

The variations in the $Q^*_a(440)$ vs. Tchl *a* relationship were also clearly different between the TS and ECS (Fig. 4a). The $Q^*_a(440)$ of surface and SCM waters from the TS were inversely correlated with Tchl *a* ($P < 0.01$, $R^2 = 0.704$), but such a correlation was not observed in the ECS ($P = 0.27$, $R^2 = 0.011$). These differences were consistent with those of the $a^*_{ph}(440)$ vs. Tchl *a* relationship in the TS and ECS (Fig. 3c).

BGD
10, 14475–14514, 2013

In this study, phytoplankton cell size was not measured directly, relationships between $Q_a^*(440)$ and the size-fractions of micro-, nano-, and pico-phytoplankton for all samples were investigated to assess the effects of cell size on $Q_a^*(440)$ (Fig. 4b–d). The $Q_a^*(440)$ displayed a tendency to significantly decrease and increase with the increase in the micro- ($P < 0.01$, $R^2 = 0.436$) and pico-phytoplankton fractions ($P < 0.01$, $R^2 = 0.309$), respectively. There was no significant correlation between $Q_a^*(440)$ and the nano-phytoplankton fraction ($P = 0.02$, $R^2 = 0.036$). The samples were dominated by the micro-, nano-, and pico-phytoplankton (fraction > 0.45) with clearly different average $Q_a^*(440)$ values of 0.46, 0.64, and 0.74, respectively.

3.5 Variations in phytoplankton size classes estimated from pigments identified by HPLC

The size structure of algal populations was clearly different among samples from the TS_S, TS_SCM, ECS_S, and ECS_SCM (Fig. 5 and Table 3). The most oligotrophic waters from the TS_S were characterized by a high fraction of pico-phytoplankton (average of 0.54) and low fractions both for micro- (average of 0.14) and nano-phytoplankton (average of 0.32). However, the pico-phytoplankton fractions of TS_SCM were extremely low, with a range from 0.00 to 0.13, while micro- (range: 0.23–0.85) and nano-phytoplankton (range: 0.14–0.72) had high average fractions of 0.58 and 0.39, respectively. The ECS_S contained mixed populations, and the fractions of micro-, nano-, and pico-phytoplankton ranged from 0.00–0.75 (average of 0.26), from 0.13–0.73 (average of 0.39), and from 0.05–0.84 (average of 0.34), respectively. Most of the samples from the ECS_SCM contained an abundance of nano-phytoplankton (average fraction of 0.50), while fraction of pico-phytoplankton was also considerable (range: 0.02–0.51, average value of 0.19). Interpreting HPLC pigment data, those pico-phytoplankton in the ECS_S and ECS_SCM might be cyanobacteria.

The variations in the phytoplankton size-fractions as a function of Tchl *a* were also different in the TS and ECS (Fig. 6). Size-fractions in the TS displayed a clear rela-

BGD
10, 14475–14514, 2013

tionship with Tchl *a* (Fig. 6a). The micro-phytoplankton fraction increased as the Tchl *a* increased, and they became the dominant algal population (> 0.45) when Tchl *a* levels were around 0.90 mg m^{-3}. The pico-phytoplankton fraction decreased with an increase in Tchl *a*, with a steep decrease at Tchl *a* levels of around 0.58 mg m^{-3}, and becoming very low (< 0.05) at Tchl *a* levels greater than 0.80 mg m^{-3}. Nano-phytoplankton were abundant at medium Tchl *a* levels, with a maximum fraction of 0.54 at Tchl *a* levels around 0.78 mg m^{-3}. However, these relationships between the size-fraction and Tchl *a* were not observed in the ECS (Fig. 6b).

3.6 Variations in phytoplankton pigment composition

Accessory pigments were classified into four groups (Bricaud et al., 2004): (1) photoprotective carotenoids (PPC) including zeaxanthin, diadinoxanthin, alloxanthin, carotenes, violaxanthin, and lutein; (2) photosynthetic carotenoids (PSC) including fucoxanthin, peridinin, 19′-butanoyloxyfucoxanthin, and 19′-hexanoyloxyfucoxanthin; (3) total Chl *b* (Tchl *b*) as the sum of Chl *b* and divinyl Chl *b*; and (4) total chlorophyll *c* (Tchl *c*) as the sum of chlorophyll c_1, c_2, and c_3. The four groups of accessory pigments were then normalized by Tchl *a* (Fig. 7). The ratio of PPC to Tchl *a* was higher in surface waters than in SCM waters in both the TS and ECS. The ratio of PSC to Tchl *a* had a relatively uniform distribution between the surface and SCM waters in the ECS but there was a large difference in the TS, and the ratio in the TS_S was relatively higher than in the ECS_S. The distribution of Tchl *b*/Tchl *a* ratios displayed no clear characteristics. The Tchl *c*/Tchl *a* ratio in the TS_S was almost 0, while in the ECS_S it was similar to in the ECS_SCM. The Tchl *c*/Tchl *a* ratios in the TS_SCM were higher than in the ECS_SCM.

The diversity of pigment composition caused small but significant variations in the $a^*_{pigm}(440)$ (Fig. 8). The linear regression analysis between $a^*_{ph}(440)$ and $a^*_{pigm}(440)$ in all samples indicated that 35.1 % of the variation in $a^*_{ph}(440)$ could be explained by $a^*_{pigm}(440)$ (Fig. 8a). The corresponding contributions for TS and ECS were 45.7 % and

BGD
10, 14475–14514, 2013

39.1 %, respectively. In addition, $a^*_{pigm}(440)$ had a weak power correlation with Tchl *a* ($P = 0.02$, $R^2 = 0.218$) in the TS, and a very poor correlation in the ECS ($P = 0.04$, $R^2 = 0.037$) (Fig. 8b). The variability in $a^*_{pigm}(675)$ was smaller than that in $a^*_{pigm}(440)$ (data not shown). A linear regression analysis between $a^*_{ph}(675)$ and $a^*_{pigm}(675)$ revealed that the pigment composition was responsible for only 13.2 % of the variation in $a^*_{ph}(675)$, which confirmed that the main variation of $a^*_{ph}(\lambda)$ originated from the packaging effect. The larger contribution of $a^*_{pigm}(440)$ to the variation of $a^*_{ph}(440)$ than $a^*_{ph}(675)$ explained why $a_{ph}(440)$ vs. Tchl *a* was more scattered than $a_{ph}(675)$ vs. Tchl *a* (Fig. 3a and b).

Values of $a^*_{pigm}(440)$ were similar in the ECS_S and TS_S with averages and standard deviations of $0.060 \pm 0.008\,m^2\,mg^{-1}$ and $0.064 \pm 0.007\,m^2\,mg^{-1}$, respectively. Values were also similar in the ECS_SCM ($0.054 \pm 0.004\,m^2\,mg^{-1}$) and TS_SCM ($0.060 \pm 0.004\,m^2\,mg^{-1}$). The difference in $a^*_{pigm}(440)$ between the ECS_S and ECS_SCM was significant (Kolmogorov–Smirnov test, $P < 0.01$), but was not significant between the TS_S and TS_SCM (Kolmogorov–Smirnov test, $P = 0.31$).

4 Discussion

4.1 General factors influencing phytoplankton light absorption

The packaging effect and pigment composition are the two main causes of the variations in $a^*_{ph}(\lambda)$ (Morel and Bricaud, 1981; Bricaud et al., 1995). Of the two factors, the packaging effect is considered to be the dominant cause of variability in $a^*_{ph}(\lambda)$ (Morel and Bricaud, 1981; Stuart et al., 1998). This was confirmed in the present study by the high correlation between $a^*_{ph}(440)$ and $Q^*_a(440)$ in all samples. Linear regression analyses between $a^*_{pigm}(\lambda)$ and $a^*_{ph}(\lambda)$ at both 440 nm and 675 nm also indicated the dominance of the packaging effect in causing variability in $a^*_{ph}(\lambda)$ (Fig. 8a). These results agree with those of Stuart et al. (1998) who also used a multiple regression analysis between $a^*_{ph}(440)$ and the concentrations of all the major pigments normalized to

BGD
10, 14475–14514, 2013

Chl *a*, and suggested that 58 % to 71 % of variability in $a^*_{ph}(440)$ could be explained by the packaging effect.

In turn, phytoplankton cell size is considered to have a key role in the determination of the packaging effect (Morel and Bricaud, 1981; Ciotti et al., 2002; Zhang et al., 2012). It is well known that large phytoplankton produce a strong packaging effect, which results in low $a^*_{ph}(\lambda)$, while the $a^*_{ph}(\lambda)$ of small phytoplankton is high because of the lower packaging effect (Stuart et al., 1998; Babin et al., 2003). Ciotti et al. (2002) stated that differences in the phytoplankton cell size were responsible for more than 80 % of the variability in the absorption spectrum. Bricaud et al. (2004) also reported that change in the phytoplankton size structure was the main factor leading to variations in $a^*_{ph}(\lambda)$ through the packaging effect. Costa Goela et al. (2013) stated that the packaging effect could be evaluated by the $a_{ph}(440)/a_{ph}(678)$ ratio, and found that this ratio was negatively correlated with the micro-phytoplankton fraction and positively correlated with the nano- and pico-phytoplankton fractions. In this study, the relationships between $Q^*_a(440)$ and the phytoplankton size-fractions estimated from HPLC pigment data for all samples indicated that the packaging effect increased and decreased when micro- and pico-phytoplankton become abundant, respectively (Fig. 4b–d), which is consistent with the results of Costa Goela et al. (2013).

Note that the intracellular pigment concentration, which usually changes with light conditions due to photo-acclimation, also affects the $a^*_{ph}(\lambda)$ through the packaging effect in the same way as cell size (Morel and Bricaud, 1981). Lohrenz et al. (2003) reported that the packaging effect clearly operated even when the cell size was smaller than 3 µm in SCM samples from west Florida. Babin et al. (2003) also suggested that the $a^*_{ph}(\lambda)$ was relatively low in deep waters, despite small cell size, because of the high intracellular pigment concentration, which generated some packaging effect. The dataset collected in this study incorporated SCM samples from the TS and ECS, which might both possess high intracellular pigment concentrations as an adaption to the low irradiance conditions. Even in surface waters, the intracellular pigment concentration is variable due to changes in light conditions (Bricaud et al., 2004). Therefore, although

BGD
10, 14475–14514, 2013

phytoplankton cell size seems a key factor controlling the $a^*_{ph}(\lambda)$ through the packaging effect in our study, the intracellular pigment concentration may be another factor causing variations in $a^*_{ph}(\lambda)$, especially between the surface and SCM.

4.2 Differences of phytoplankton absorption and its influencing factors between the ECS and TS

Our results revealed a clear difference in salinity and the phytoplankton bio-optical properties between the ECS_S and TS_S. The low salinity (< 32) in the ECS_S and the relatively high salinity (> 32) in the TS_S confirmed the strong and weak influence of Changjiang fresh water on the ECS_S and TS_S, respectively (Fig. 3). The low-salinity waters of the ECS_S indicate that there is a higher Tchl *a* than in the TS_S (Table 2), which agrees with the results of Yamaguchi et al. (2012) who suggested that the CDW could enhance Chl *a* in the ECS_S. As a consequence, a higher $a_{ph}(\lambda)$ was observed in the ECS_S than in the TS_S (Figs. 2 and 3). However, the $a^*_{ph}(\lambda)$ in the ECS_S was lower on average than in the TS_S (Figs. 2 and 3). Comparisons of the packaging effect and $a^*_{pigm}(440)$ indicated a slightly lower $Q^*_a(440)$ in the ECS_S than in the TS_S and a similar $a^*_{pigm}(440)$ between the ECS_S and TS_S (Figs. 4a and 8). These results suggest that the difference in $a^*_{ph}(\lambda)$ between the ECS_S and TS_S may be primarily caused by the packaging effect. The phytoplankton size structure revealed that the stronger packaging effect in the ECS_S may be caused by increase of large phytoplankton (Figs. 5 and 6). It should be noted that though the $a^*_{ph}(\lambda)$ was generally lower in the ECS_S than in the TS_S, the majority of low-salinity water in the ECS_S had much higher values than those produced by the regressions of Bricaud et al. (1995) (Fig. 3). From Fig. 6b, it can be seen that pico-phytoplankton which might be cyanobacteria were still abundant in the ECS_S, even though Tchl *a* was high. This result contradicts previous studies, which have indicated that small and large cells are abundant in low- and high-Chl *a* waters, respectively (Brewin et al., 2010; Hirata et al.,

BGD
10, 14475–14514, 2013

2011). The abundance of pico-phytoplankton in the ECS_S may result in a higher $a^*_{ph}(\lambda)$ than the values from the regressions of Bricaud et al. (1995).

The ECS_SCM also differed from TS_SCM. Most ECS_SCM samples were taken from waters beneath the CDW, and these samples also had a lower local salinity than those taken from the TS_SCM, implying that ECS_SCM was to some extent influenced by the CDW. The average Tchl *a* of the ECS_SCM was nearly twice as high as that of the TS_SCM, and the average $a_{ph}(\lambda)$ of the ECS_SCM was almost three times larger than that of the TS_SCM (Table 2). As a result, the $a^*_{ph}(\lambda)$ was much higher in the ECS_SCM than in the TS_SCM. By comparing the packaging effect (cell size) and $a^*_{pigm}(440)$, we found that the packaging effect (cell size) was the main cause for the differences in $a^*_{ph}(\lambda)$ between the ECS_SCM and TS_SCM (Figs. 4a and 8). The ECS_SCM was generally characterized by an abundance of large phytoplankton, while pico-phytoplankton which might be cyanobacteria still composed considerable fractions (Figs. 5 and 6). However, the high-salinity waters in the TS_SCM indicated a low abundance of pico-phytoplankton, with large phytoplankton being dominant. Finally, the small cells might generate a higher $a^*_{ph}(\lambda)$ in the ECS_SCM than in the TS_SCM. In addition, as with the ECS_S, the $a^*_{ph}(\lambda)$ in the ECS_SCM was also higher than the values produced by the regression of Bricaud et al. (1995) (Fig. 3), which might be because of the relatively abundant pico-phytoplankton. These findings indicate that the ECS_SCM was also influenced by the CDW, and this influence was reflected by the considerable pico-phytoplankton and relatively high $a^*_{ph}(\lambda)$ in the ECS_SCM.

A clear difference was found in $a^*_{ph}(\lambda)$ between the TS_S and TS_SCM, but no such difference was obvious between the ECS_S and ECS_SCM (Figs. 2 and 3). The difference in the packaging effect between the TS_S and TS_SCM was significant (Fig. 4a), while the $a^*_{pigm}(\lambda)$ was very similar in the two layers, although the proportions of pigment groups present were quite different (Figs. 7 and 8). This result is consistent with those of Bricaud et al. (2004), who suggested that even if the variations in the pigment composition were large, the effects of various pigments on absorption might be compensated for, so that the actual influence of pigment composition on $a^*_{ph}(\lambda)$ was ulti-

BGD
10, 14475–14514, 2013

mately reduced. These findings indicated that the significant vertical variation of $a^*_{ph}(\lambda)$ in the TS was mainly driven by the packaging effect (cell size). However, in the ECS, both the packaging effect (cell size) and $a^*_{pigm}(440)$ were similar in the surface and SCM (Figs. 4a, 5, 6, and 8). These factors eventually resulted in a small vertical variation in $a^*_{ph}(\lambda)$ in the ECS.

It is well known that phytoplankton community structure is related to local nutrient availability. Oligotrophic and eutrophic waters are dominated by small and large phytoplankton, respectively (Stæhr et al., 2004; Uitz et al., 2008). Consistently, oligotrophic waters in the TS_S were dominated by pico-phytoplankton, and micro-phytoplankton dominated in the TS_SCM where the nutrients were abundant (unpublished data). For the ECS, large amounts of nitrogen were supplied by the CDW to the shelf area during summer (Gong et al., 1996), which was expected to induce the large phytoplankton-dominated structure. However, despite of the sufficient nutrients, significant numbers of pico-phytoplankton (cyanobacteria) were still found in the ECS_S as well as in the ECS_SCM in this study. This phenomenon may be related to the nutrient structure. Herbland et al. (1998) found that waters in the shelf of the south Bay of Biscay with high N/P ratios were dominated by pico-phytoplankton (< 3 µm, proportion ranged from 40 % to 70 %). The previous studies also found that the N/P ratios were high in the ECS_S and ECS_SCM, particularly in the western part of the ECS_S (unpbulbished data; Wang et al., 2003; Zhang et al., 2007). These findings imply that the N/P ratio may be an important factor influencing the phytoplankton size structure in the ECS.

4.3 Correlations among Tchl *a*, phytoplankton size-fraction, and Tchl *a*-specific absorption coefficient

For the global ocean, micro-phytoplankton are abundant in high-Chl *a* waters and their fraction increases with an increase in Chl *a*. In contrast, pico-phytoplankton prevail in low-Chl *a* waters and their fraction decreases with an increase in Chl *a*, while nano-phytoplankton dominate in medium-Chl *a* waters (Kameda and Ishizaka, 2005; Brewin et al., 2010). According to our study, variations in the phytoplankton size classes in

BGD
10, 14475–14514, 2013

the TS were similar to those reported by Brewin et al. (2010). This suggests that the TS possess the typical characteristics of the global ocean, and implies that the size-based two or three population absorption models (Sathyendranath et al., 2001; Devred et al., 2006, 2011; Brewin et al., 2011) and the size-fraction estimation models (Uitz et al., 2006; Brewin et al., 2010; Hirata et al., 2011), which were proposed based on the correlations of size-fractions with Chl *a* in the global ocean, could be adapted for the TS. However, in the ECS there were no clear tendencies noted in the variations of size-fractions vs. Tchl *a*. When we applied the model of Hirata et al. (2011) in the ECS, the relative RMSEs between model-retrieved and HPLC-estimated fractions for micro-, nano- and pico-phytoplankton were 338.0 %, 66.9 % and 103.8 %, respectively. At high Tchl *a* range, the model-retrieved fractions displayed clear overestimation and underestimation for micro- and pico-phytoplankton, respectively. These findings indicate that the models mentioned above may not be applicable to the ECS.

Bricaud et al. (1995) found that the $a^*_{ph}(\lambda)$ was negatively correlated with Chl *a* in the global ocean, and these correlations were very stable even when subsurface samples were incorporated. In this study, consistent negative correlations between $a^*_{ph}(\lambda)$ and Tchl *a* with those of Bricaud et al. (1995) were observed in the TS, but not in the ECS (Fig. 3c and d). The factors responsible for these differences between the TS and ECS can be clearly seen in Fig. 9. In the TS, $Q^*_a(440)$, which played a leading role in determining $a^*_{ph}(440)$, was strongly correlated with Tchl *a*, whereas $a^*_{pigm}(440)$ had a relatively weak correlation with Tchl *a*. This implies that the significant correlation with a power function for $a^*_{ph}(440)$ with Tchl *a* was mainly driven by the $Q^*_a(440)$. The significant correlation between $Q^*_a(440)$ and Tchl *a* was primarily controlled by the cell-size variations by the fact that pico-phytoplankton with a large $Q^*_a(440)$ dominated at low Tchl *a*, nano-phytoplankton with moderate $Q^*_a(440)$ at medium Tchl *a*, and micro-phytoplankton with small $Q^*_a(440)$ at high Tchl *a*. However, in the ECS, the phytoplankton size-fractions displayed irregular trends, which resulted in a poor correlation between $Q^*_a(440)$ and Tchl *a*. The $a^*_{pigm}(440)$ was also not correlated with Tchl *a*. Due to the influence of these factors, $a^*_{ph}(440)$ was poorly correlated with Tchl *a*.

BGD
10, 14475–14514, 2013

Babin et al. (2003) pointed out that the specific parameterizations for the global ocean, such as the relationships between $a_{ph}(\lambda)$ and Chl *a*, might not necessarily hold in coastal waters. They found that if they merged data from all of the coastal regions, most of the $a_{ph}(\lambda)$ vs. Chl *a* data displayed a similar tendency to that established in the global ocean by Bricaud et al. (1995). However, some samples did depart from the regression undertaken by Bricaud et al. (1995). Most of the samples from the ECS also displayed obvious departures from the regression of Bricaud et al. (1995), especially at high Tchl *a* (Fig. 3), which was consistent with the findings of Babin et al. (2003). In addition to the findings of Babin et al. (2003), our study implies that not only the specific parameterizations for the global ocean may become invalid, but even the correlation between $a^*_{ph}(\lambda)$ and Chl *a* may not exist in some coastal regions.

It should be noted that samples from the ECS that deviated from the regressions of Bricaud et al. (1995) were mainly taken from the low-salinity CDW (< 32) and the SCM waters beneath them (Fig. 3). These outliers had a higher $a^*_{ph}(\lambda)$ and a larger variability at the same Tchl *a* than those in the TS and the global regressions, which resulted in a poor correlation between $a^*_{ph}(\lambda)$ and Tchl *a*. However, it should also be noted that some samples from the ECS_S with high surface salinity (> 32) and samples from the ECS_SCM beneath them followed similar trends to the TS and the global regressions (Fig. 3). These results imply that the departure of the ECS samples from the global regressions as well as the poor correlation between $a^*_{ph}(\lambda)$ and Tchl *a* may be influenced by the Changjiang fresh water.

5 Conclusions

In this study, the influence of fresh water on phytoplankton light absorption properties was studied in the East China Sea by comparison with the Tsushima Strait. Our analysis showed that the freshwater discharge could significantly change the size structure at the surface, and even in the subsurface chlorophyll *a* maximum. The discharge also generated absorption characteristics that were distinctly different from those of the

BGD
10, 14475–14514, 2013

global ocean. At the same Tchl *a* range, most of samples influenced by fresh water had a high magnitude and large variability of $a^*_{ph}(\lambda)$.

By combining the surface and subsurface chlorophyll *a* maximum samples, the Tsushima Strait displayed consistent patterns of size-fraction changing with Tchl *a* and correlations between $a^*_{ph}(\lambda)$ and Tchl *a* with those established in the global ocean. However, such characteristics were not found in the East China Sea, probably due to the influence of Changjiang freshwater. These findings provide evidence that the correlation between Tchl *a* with phytoplankton size classes as well as $a^*_{ph}(\lambda)$, which have been observed in the global ocean, may become invalid in coastal regions because of the freshwater discharge and possibly high N/P ratio. We suggest that more attention should be given to applying the models proposed based on the general relationship between $a^*_{ph}(\lambda)$ and Tchl *a* and on the patterns of size-fractions changing with Tchl *a* in regions influenced by fresh water.

Acknowledgements. We would like to thank the captains, officers and crews of T/V *Nagasaki maru* and R/V *Tansei maru* for excellent assistance during field sampling and measurements. This research was partly supported by the Second-generation Global Imager project of the Japan Aerospace Exploration Agency. The English in this document has been checked by at least two professional editors, both native speakers of English. For a certificate, please see: http://www.textcheck.com/certificate/Tnh5oz.

References

Babin, M., Therriault, J. C., Legendre, L., and Condal, A.: Variations in the specific absorption coefficient for natural phytoplankton assemblages: impact on estimates of primary production, Limnol. Oceanogr., 38, 154–177, 1993.

Babin, M., Stramski, D., Ferrari, G. M., Claustre, H., Bricaud, A., Obolensky, G., and Hoepffner, N.: Variations in the light absorption coefficients of phytoplankton, nonalgal particles, and dissolved organic matter in coastal waters around Europe, J. Geophys. Res., 108, 3211, doi:10.1029/2001jc000882, 2003.

BGD
10, 14475–14514, 2013

Barlow, R., Aiken, J., Holligan, P., Cummings, D., Maritorena, S., and Hooker, S.: Phytoplankton pigment and absorption characteristics along meridional transects in the Atlantic Ocean, Deep-Sea Res. Pt. I, 49, 637–660, 2002.
Brewin, R. J., Sathyendranath, S., Hirata, T., Lavender, S. J., Barciela, R. M., and Hardman-Mountford, N. J.: A three-component model of phytoplankton size class for the Atlantic Ocean, Ecol. Model., 221, 1472–1483, 2010.
Brewin, R. J., Devred, E., Sathyendranath, S., Lavender, S. J., and Hardman-Mountford, N. J.: Model of phytoplankton absorption based on three size classes, Appl. Optics, 50, 4535–4549, 2011.
Bricaud, A., Babin, M., Morel, A., and Claustre, H.: Variability in the chlorophyll-specific absorption coefficients of natural phytoplankton: analysis and parameterization, J. Geophys. Res., 100, 13321–13332, 1995.
Bricaud, A., Claustre, H., Ras, J., and Oubelkheir, K.: Natural variability of phytoplanktonic absorption in oceanic waters: influence of the size structure of algal populations, J. Geophys. Res., 109, C11010, doi:10.1029/2004jc002419, 2004.
Brunelle, C. B., Larouche, P., and Gosselin, M.: Variability of phytoplankton light absorption in Canadian Arctic seas, J. Geophys. Res., 117, C00G17, doi:10.1029/2011jc007345, 2012.
Ciotti, A. M. and Bricaud, A.: Retrievals of a size parameter for phytoplankton and spectral light absorption by colored detrital matter from water-leaving radiances at SeaWiFS channels in a continental shelf region off Brazil, Limnol. Oceanogr.-Meth., 4, 237–253, 2006.
Ciotti, A. M., Lewis, M. R., and Cullen, J. J.: Assessment of the relationships between dominant cell size in natural phytoplankton communities and the spectral shape of the absorption coefficient, Limnol. Oceanogr., 47, 404–417, 2002.
Cleveland, J. S.: Regional models for phytoplankton absorption as a function of chlorophyll *a* concentration, J. Geophys. Res., 100, 13333–13344, 1995.
Cleveland, J. and Weidemann, A.: Quantifying absorption by aquatic particles: a multiple scattering correction for glass-fiber filters, Limnol. Oceanogr., 38, 1321–1327, 1993.
Costa Goela, P., Icely, J., Cristina, S., Newton, A., Moore, G., and Cordeiro, C.: Specific absorption coefficient of phytoplankton off the Southwest coast of the Iberian Peninsula: a contribution to algorithm development for ocean colour remote sensing, Cont. Shelf Res., 52, 119–132, doi:10.1016/j.csr.2012.11.009, 2013.

BGD
10, 14475–14514, 2013

Devred, E., Sathyendranath, S., Stuart, V., Maass, H., Ulloa, O., and Platt, T.: A two-component model of phytoplankton absorption in the open ocean: theory and applications, J. Geophys. Res., 111, C03011, doi:10.1029/2005JC002880, 2006.

Devred, E., Sathyendranath, S., Stuart, V., and Platt, T.: A three component classification of phytoplankton absorption spectra: application to ocean-color data, Remote Sens. Environ., 115, 2255–2266, 2011.

Garver, S. A. and Siegel, D. A.: Inherent optical property inversion of ocean color spectra and its biogeochemical interpretation, 1. Time series from the Sargasso Sea, J. Geophys. Res., 102, 18607–18625, 1997.

Gong, G. C., Lee Chen, Y. L., and Liu, K. K.: Chemical hydrography and chlorophyll *a* distribution in the East China Sea in summer: implications in nutrient dynamics, Cont. Shelf Res., 16, 1561–1590, 1996.

Gordon, H. R., Brown, O. B., Evans, R. H., Brown, J. W., Smith, R. C., Baker, K. S., and Clark, D. K.: A semianalytic radiance model of ocean color, J. Geophys. Res., 93, 10909–10924, 1988.

Guo, X., Miyazawa, Y., and Yamagata, T.: The Kuroshio onshore intrusion along the shelf break of the East China Sea: the origin of the Tsushima Warm Current, J. Phys. Oceanogr., 36, 2205–2231, 2006.

Hama, T., Shin, K., and Handa, N.: Spatial variability in the primary productivity in the East China Sea and its adjacent waters, J. Oceanogr., 53, 41–51, 1997.

Harimoto, T., Ishizaka, J., and Tsuda, R.: Latitudinal and vertical distributions of phytoplankton absorption spectra in the central North Pacific during spring 1994, J. Oceanogr., 55, 667–679, 1999.

He, M. X., Liu, Z. S., Du, K. P., Li, L. P., Chen, R., Carder, K. L., and Lee, Z. P.: Retrieval of chlorophyll from remote-sensing reflectance in the China seas, Appl. Optics, 39, 2467–2474, 2000.

Herbland, A., Delmas, D., Laborde, P., Sautour, B., and Artigas, F.: Phytoplankton spring bloom of the Gironde plume waters in the Bay of Biscay: early phosphorus limitation and food-web consequences, Oceanol. Acta, 21, 279–291, 1998.

Hirata, T., Aiken, J., Hardman-Mountford, N., Smyth, T., and Barlow, R.: An absorption model to determine phytoplankton size classes from satellite ocean colour, Remote Sens. Environ., 112, 3153–3159, 2008.

BGD
10, 14475–14514, 2013

Hirata, T., Hardman-Mountford, N. J., Brewin, R. J. W., Aiken, J., Barlow, R., Suzuki, K., Isada, T., Howell, E., Hashioka, T., Noguchi-Aita, M., and Yamanaka, Y.: Synoptic relationships between surface Chlorophyll *a* and diagnostic pigments specific to phytoplankton functional types, Biogeosciences, 8, 311–327, doi:10.5194/bg-8-311-2011, 2011.

Hoge, F. E., Wright, C. W., Lyon, P. E., Swift, R. N., and Yungel, J. K.: Satellite retrieval of the absorption coefficient of phytoplankton phycoerythrin pigment: theory and feasibility status, Appl. Optics, 38, 7431–7441, 1999.

Ishizaka, J.: Spatial distribution of primary production off Sanriku, northwestern Pacific, during spring estimated by Ocean Color and Temperature Scanner (OCTS), J. Oceanogr., 54, 553–564, 1998.

Isobe, A., Ando, M., Watanabe, T., Senjyu, T., Sugihara, S., and Manda, A.: Freshwater and temperature transports through the Tsushima-Korea Straits, J. Geophys. Res., 107, C73065, doi:10.1029/2000jc000702, 2002.

Kameda, T. and Ishizaka, J.: Size-fractionated primary production estimated by a two-phytoplankton community model applicable to ocean color remote sensing, J. Oceanogr., 61, 663–672, 2005.

Kishino, M., Takahashi, M., Okami, N., and Ichimura, S.: Estimation of the spectral absorption coefficients of phytoplankton in the sea, B. Mar. Sci., 37, 634–642, 1985.

Lohrenz, S. E., Weidemann, A. D., and Tuel, M.: Phytoplankton spectral absorption as influenced by community size structure and pigment composition, J. Plankton Res., 25, 35–61, 2003.

Matsuoka, A., Hill, V., Huot, Y., Babin, M., and Bricaud, A.: Seasonal variability in the light absorption properties of western Arctic waters: parameterization of the individual components of absorption for ocean color applications, J. Geophys. Res., 116, C02007, doi:10.1029/2009jc005594, 2011.

Mitchell, B. G.: Algorithms for determining the absorption coefficient for aquatic particulates using the quantitative filter technique, in: SPIE. Ocean Opt. X, Orlando, USA, 1 September 1990, 1302, 137–148, 1990.

Morel, A.: Optical modeling of the upper ocean in relation to its biogenous matter content (case I waters), J. Geophys. Res., 93, 10749–10768, 1988.

Morel, A. and Bricaud, A.: Theoretical results concerning light absorption in a discrete medium, and application to specific absorption of phytoplankton, Deep-Sea Res. Pt. I, 28, 1375–1393, 1981.

BGD
10, 14475–14514, 2013

Morimoto, A., Takikawa, T., Onitsuka, G., Watanabe, A., Moku, M., and Yanagi, T.: Seasonal variation of horizontal material transport through the eastern channel of the Tsushima Straits, J. Oceanogr., 65, 61–71, 2009.
Platt, T. and Sathyendranath, S.: Oceanic primary production: estimation by remote sensing at local and regional scales, Science, 241, 1613–1620, 1988.
Sathyendranath, S., Cota, G., Stuart, V., Maass, H., and Platt, T.: Remote sensing of phytoplankton pigments: a comparison of empirical and theoretical approaches, Int. J. Remote Sens., 22, 249–273, doi:10.1080/014311601449925, 2001.
Siswanto, E., Nakata, H., Matsuoka, Y., Tanaka, K., Kiyomoto, Y., Okamura, K., Zhu, J., and Ishizaka, J.: The long-term freshening and nutrient increases in summer surface water in the northern East China Sea in relation to Changjiang discharge variation, J. Geophys. Res., 113, C10030, doi:10.1029/2008jc004812, 2008.
Stæhr, P., Markager, S., and Sand-Jensen, K.: Pigment specific in vivo light absorption of phytoplankton from estuarine, coastal and oceanic waters, Mar. Ecol.-Prog. Ser., 275, 115–128, 2004.
Stuart, V., Sathyendranath, S., Platt, T., Maass, H., and Irwin, B. D.: Pigments and species composition of natural phytoplankton populations: effect on the absorption spectra, J. Plankton Res., 20, 187–217, 1998.
Suzuki, K., Kishino, M., Sasaoka, K., Saitoh, S., and Saino, T.: Chlorophyll-specific absorption coefficients and pigments of phytoplankton off Sanriku, northwestern North Pacific, J. Oceanogr., 54, 517–526, 1998.
Uitz, J., Claustre, H., Morel, A., and Hooker, S. B.: Vertical distribution of phytoplankton communities in open ocean: an assessment based on surface chlorophyll, J. Geophys. Res., 111, C08005, doi:10.1029/2005jc003207, 2006.
Uitz, J., Huot, Y., Bruyant, F., Babin, M., and Claustre, H.: Relating phytoplankton photophysiological properties to community structure on large scales, Limnol. Oceanogr., 53, 614–630, 2008.
Van Heukelem, L. and Thomas, C. S.: Computer-assisted high-performance liquid chromatography method development with applications to the isolation and analysis of phytoplankton pigments, J. Chromatogr. A, 910, 31–49, 2001.
Vidussi, F., Claustre, H., Manca, B. B., Luchetta, A., and Marty, J. C.: Phytoplankton pigment distribution in relation to upper thermocline circulation in the eastern Mediterranean Sea during winter, J. Geophys. Res., 106, 19939–19956, 2001.

BGD
10, 14475–14514, 2013

Wang, B., Wang, X., and Zhan, R.: Nutrient conditions in the Yellow Sea and the East China Sea, Estuar. Coast. Shelf S., 58, 127–136, doi:10.1016/s0272-7714(03)00067-2, 2003.
Yamaguchi, H., Kim, H. C., Son, Y. B., Kim, S. W., Okamura, K., Kiyomoto, Y., and Ishizaka, J.: Seasonal and summer interannual variations of SeaWiFS chlorophyll *a* in the Yellow Sea and East China Sea, Prog. Oceanogr., 105, 22–29, doi:10.1016/j.pocean.2012.04.004, 2012.
Zhang, J., Liu, S. M., Ren, J. L., Wu, Y., and Zhang, G. L.: Nutrient gradients from the eutrophic Changjiang (Yangtze River) Estuary to the oligotrophic Kuroshio waters and re-evaluation of budgets for the East China Sea Shelf, Prog. Oceanogr., 74, 449–478, doi:10.1016/j.pocean.2007.04.019, 2007.
Zhang, Y., Yin, Y., Wang, M., and Liu, X.: Effect of phytoplankton community composition and cell size on absorption properties in eutrophic shallow lakes: field and experimental evidence, Opt. Express, 20, 11882–11898, 2012.
Zhou, M., Shen, Z., and Yu, R.: Responses of a coastal phytoplankton community to increased nutrient input from the Changjiang (Yangtze) River, Cont. Shelf Res., 28, 1483–1489, doi:10.1016/j.csr.2007.02.009, 2008.

BGD
10, 14475–14514, 2013

Table 1. Details of the cruises where both HPLC and $a_{ph}(\lambda)$ were collected from the Tsushima Strait surface (TS_S), Tsushima Strait SCM (TS_SCM), East China Sea surface (ECS_S), and East China Sea SCM (ECS_SCM).

Cruise periods	Ship names	Locations	No. of Samples
21–26 Jul 2008	T/V *Nagasaki maru*	TS_S	13
		TS_SCM	12
8–18 Aug 2008	R/V *Tansei maru*	ECS_S	23
		ECS_SCM	24
17–27 Jul 2009	T/V *Nagasaki maru*	ECS_S	10
		ECS_SCM	2
17–27 Jul 2010	T/V *Nagasaki maru*	ECS_S	14
		ECS_SCM	3
15–25 Jul 2011	T/V *Nagasaki maru*	ECS_S	20
		ECS_SCM	22

BGD
10, 14475–14514, 2013

Table 2. Comparisons of Tchl *a*, $a_{ph}(440)$, $a_{ph}(675)$, $a^*_{ph}(440)$, $a^*_{ph}(675)$, and the ratio of $a^*_{ph}(440)$ to $a^*_{ph}(675)$ among the Tsushima Strait surface (TS_S), Tsushima Strait SCM (TS_SCM), East China Sea surface (ECS_S), and East China Sea SCM (ECS_SCM). Max: maximum; Min: minimum; Ave: average; Std: standard deviation; CV: coefficient of variation.

Variable	Location	Max	Min	Ave	Std	CV
Tchl *a*($mg\,m^{-3}$)	TS_S	0.24	0.12	0.18	0.05	26.4
	TS_SCM	3.06	0.58	1.33	0.78	58.3
	ECS_S	2.22	0.10	0.88	0.53	59.5
	ECS_SCM	6.10	0.74	2.48	1.31	52.9
$a_{ph}(440)(m^{-1})$	TS_S	0.023	0.008	0.015	0.004	27.9
	TS_SCM	0.108	0.029	0.052	0.022	41.6
	ECS_S	0.164	0.009	0.066	0.046	69.7
	ECS_SCM	0.394	0.047	0.144	0.068	47.3
$a_{ph}(675)(m^{-1})$	TS_S	0.006	0.003	0.004	0.001	25.2
	TS_SCM	0.052	0.014	0.025	0.011	46.1
	ECS_S	0.066	0.003	0.024	0.017	73.7
	ECS_SCM	0.195	0.018	0.062	0.031	49.4
$a^*_{ph}(440)(m^2\,mg^{-1})$	TS_S	0.129	0.050	0.086	0.023	26.9
	TS_SCM	0.066	0.017	0.045	0.015	32.5
	ECS_S	0.158	0.030	0.074	0.023	31.8
	ECS_SCM	0.127	0.035	0.062	0.019	30.1
$a^*_{ph}(675)(m^2\,mg^{-1})$	TS_S	0.035	0.015	0.024	0.005	19.9
	TS_SCM	0.028	0.008	0.021	0.006	28.0
	ECS_S	0.047	0.012	0.026	0.007	28.7
	ECS_SCM	0.055	0.016	0.027	0.008	29.6
$a^*_{ph}(440)/a^*_{ph}(675)$	TS_S	4.75	2.94	3.57	0.48	13.6
	TS_SCM	2.56	1.83	2.19	0.19	8.8
	ECS_S	4.60	1.80	2.91	0.52	17.8
	ECS_SCM	2.82	1.83	2.32	0.18	7.9

BGD
10, 14475–14514, 2013

Table 3. Comparisons of the Tchl *a* size-fractions of micro-, nano-, and pico-phytoplankton in the Tsushima Strait surface (TS_S), Tsushima Strait SCM (TS_SCM), East China Sea surface (ECS_S), and East China Sea SCM (ECS_SCM). Max: maximum; Min: minimum; Ave: average; Std: standard deviation; CV: coefficient of variation.

Location	Variable	Max	Min	Ave	Std	CV
TS_S	Micro	0.42	0.00	0.14	0.16	117.9
	Nano	0.59	0.00	0.32	0.15	46.2
	Pico	1.00	0.21	0.54	0.21	38.7
TS_SCM	Micro	0.85	0.23	0.58	0.21	36.6
	Nano	0.72	0.14	0.39	0.19	50.0
	Pico	0.13	0.00	0.03	0.04	107.9
ECS_S	Micro	0.75	0.00	0.26	0.20	76.7
	Nano	0.73	0.13	0.39	0.15	38.4
	Pico	0.84	0.05	0.34	0.16	47.5
ECS_SCM	Micro	0.80	0.09	0.32	0.15	46.7
	Nano	0.75	0.10	0.50	0.12	24.1
	Pico	0.51	0.02	0.19	0.11	59.1

BGD
10, 14475–14514, 2013

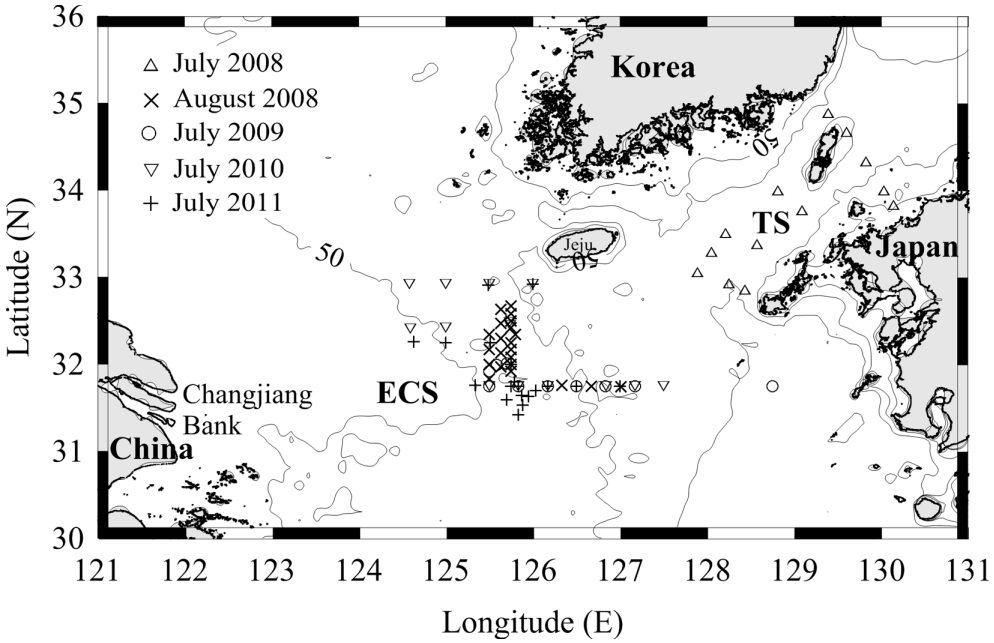

Fig. 1. Locations of the sampling stations in the Tsushima Strait (TS) in 2008 and in the East China Sea (ECS) during 2008–2011.

BGD
10, 14475–14514, 2013

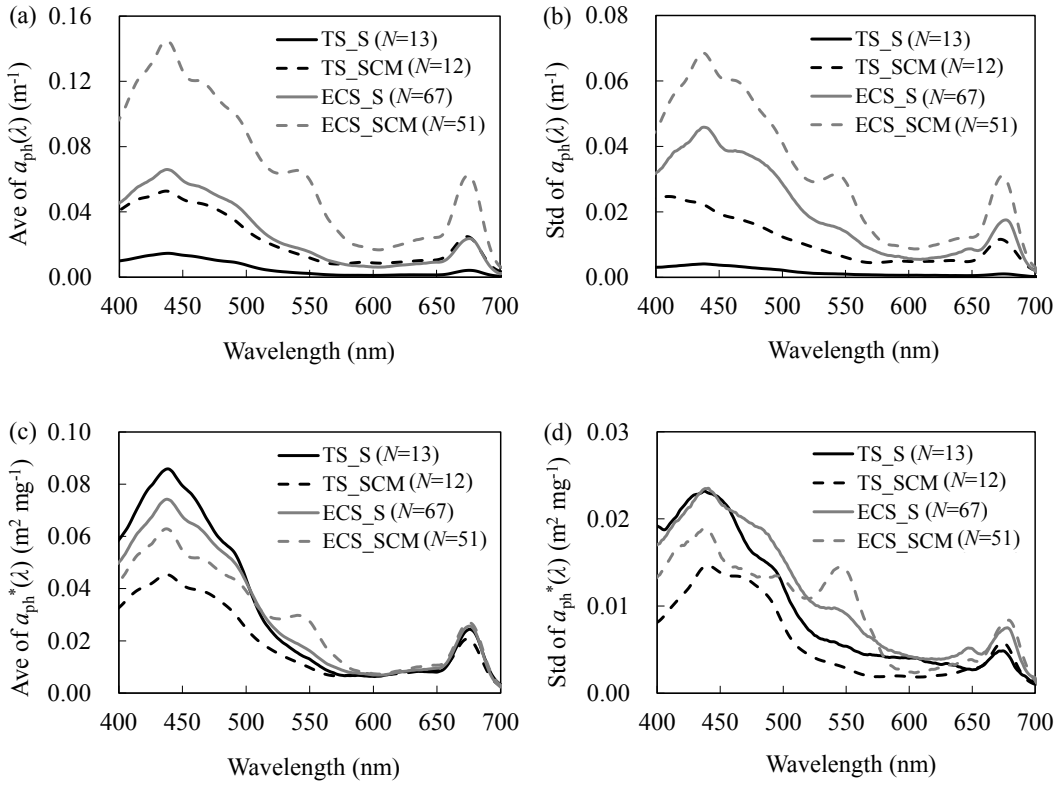

Fig. 2. Average (Ave) **(a)** and standard derivation (Std) **(b)** of $a_{ph}(\lambda)$ and Ave **(c)** and Std **(d)** of $a_{ph}^{*}(\lambda)$ in the Tsushima Strait surface (TS_S), Tsushima Strait SCM (TS_SCM), East China Sea surface (ECS_S), and East China Sea SCM (ECS_SCM).

BGD
10, 14475–14514, 2013

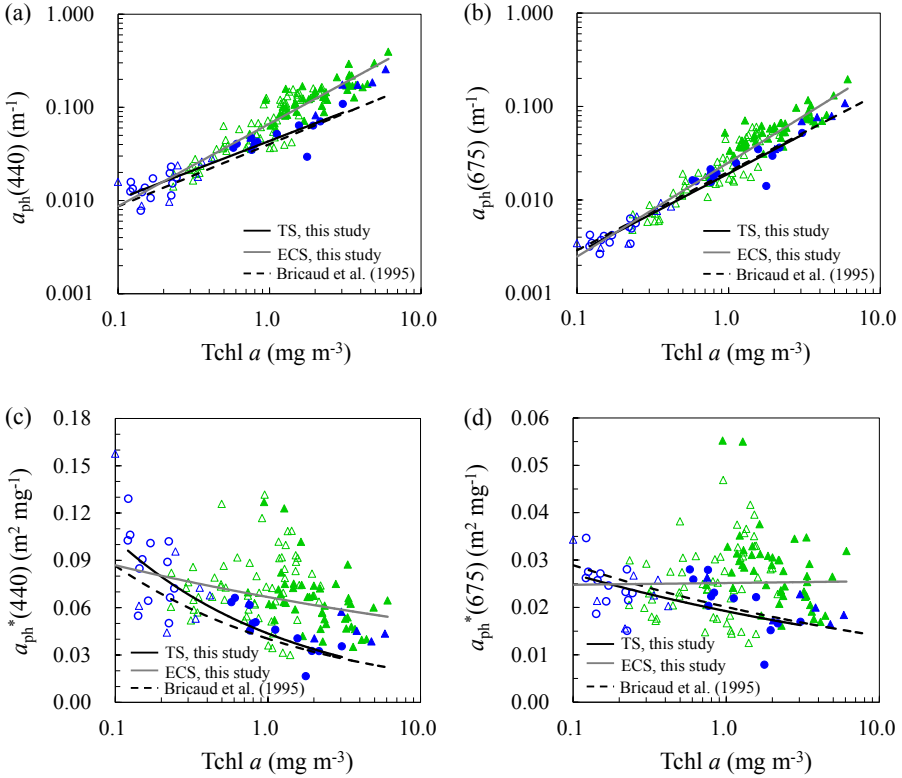

Fig. 3. Correlations between Tchl *a* and $a_{ph}(440)$ **(a)**, $a_{ph}(675)$ **(b)**, $a^*_{ph}(440)$ **(c)**, and $a^*_{ph}(675)$ **(d)**. The unfilled circle, filled circle, unfilled triangle, and filled triangle represent samples from the Tsushima Strait surface, Tsushima Strait SCM, East China Sea surface, and East China Sea SCM, respectively. Green symbols are samples with a surface salinity lower than 32, and blue symbols are samples with a surface salinity greater than 32. Black and grey lines indicate power law functions fitted in the Tsushima Strait (TS) and East China Sea (ECS), respectively. Black dashes correspond to the regressions of Bricaud et al. (1995).

BGD
10, 14475–14514, 2013

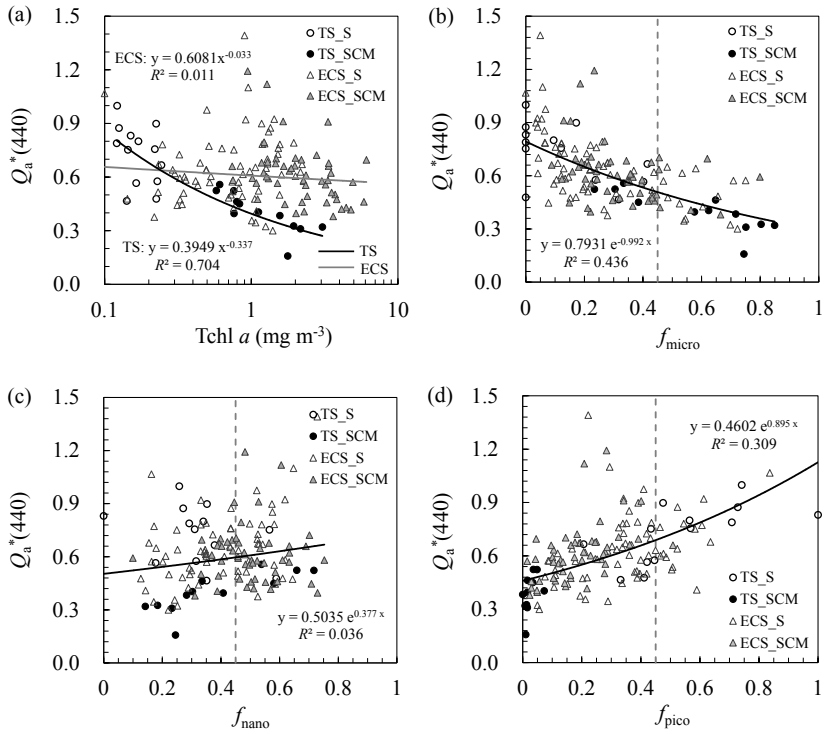

Fig. 4. Variations in $Q_a^*(440)$ as a function of Tchl *a* **(a)** and Tchl *a* size-fractions of micro- **(b)**, nano- **(c)**, and pico-phytoplankton **(d)** for samples from the Tsushima Strait surface (TS_S), Tsushima Strait SCM (TS_SCM), East China Sea surface (ECS_S), and East China Sea SCM (ECS_SCM). In **(a)**, black and grey lines indicate power law functions fitted in the Tsushima Strait (TS) and East China Sea (ECS). In **(b–d)**, black lines indicate exponential functions fitted from all samples, and grey vertical dashes are the boundaries of the dominant class with a fraction greater than 0.45.

BGD
10, 14475–14514, 2013

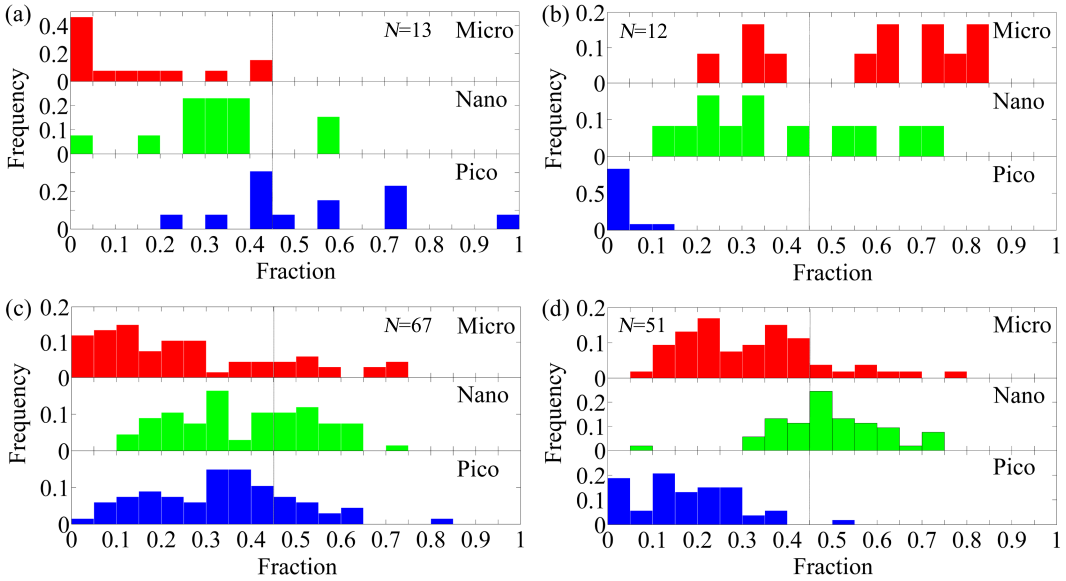

Fig. 5. Histograms showing the frequency distributions of Tchl *a* size-fractions of micro-, nano- and pico-phytoplankton in the Tsushima Strait surface **(a)**, Tsushima Strait SCM **(b)**, East China Sea surface **(c)**, and East China Sea SCM **(d)**. Grey vertical lines are the boundaries of the dominant class with a fraction greater than 0.45.

BGD
10, 14475–14514, 2013

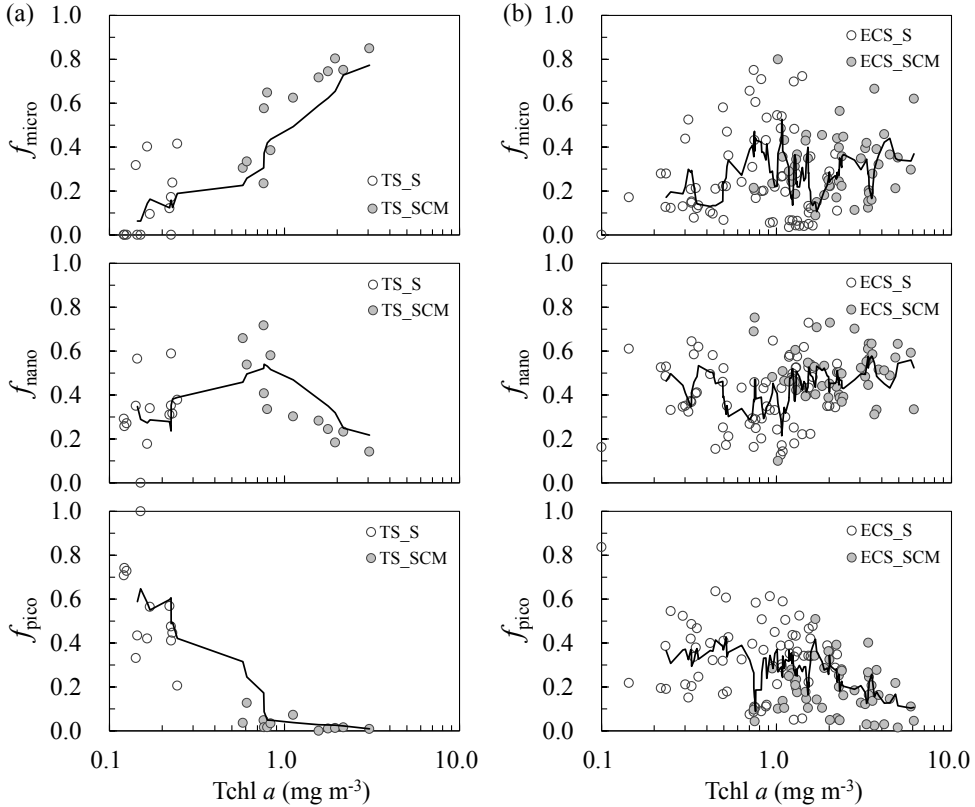

Fig. 6. Variations in Tchl *a* size-fractions of micro-, nano-, and pico-phytoplankton as a function of Tchl *a* in the Tsushima Strait (TS) **(a)** and East China Sea (ECS) **(b)**. TS_S, TS_SCM, ECS_S, and ECS_SCM represent the Tsushima Strait surface, Tsushima Strait SCM, East China Sea surface, and East China Sea SCM, respectively. Lines represent the five-point running average.

BGD
10, 14475–14514, 2013

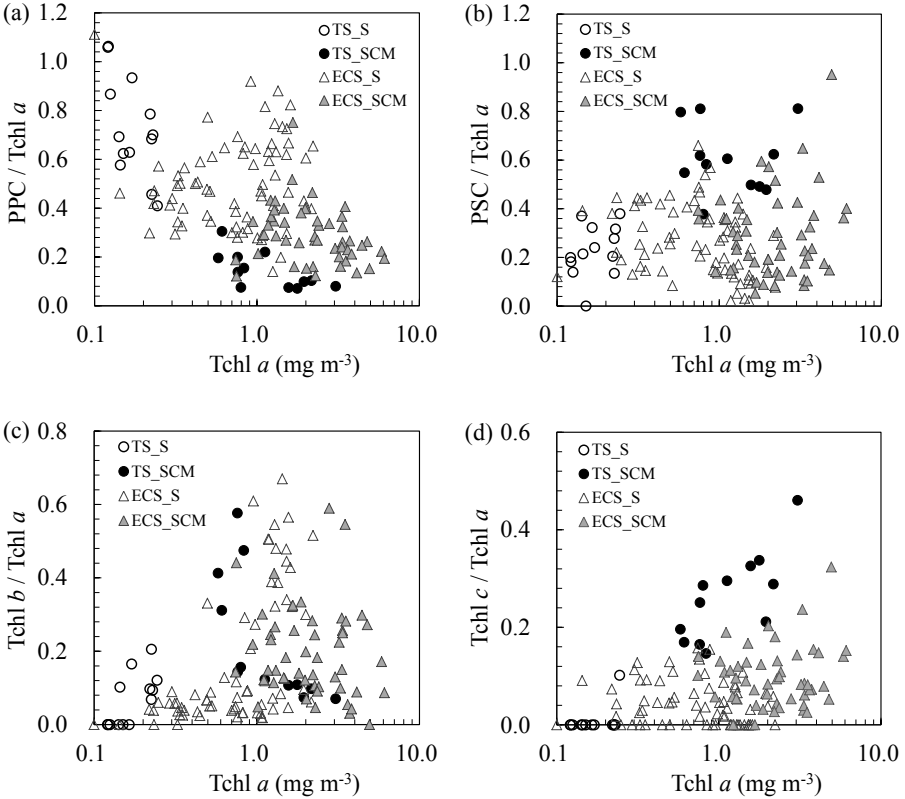

Fig. 7. Variations in the ratios of PPC **(a)**, PSC **(b)**, Tchl *b* **(c)**, and Tchl *c* **(d)** to Tchl *a* as a function of Tchl *a* in the Tsushima Strait surface (TS_S), Tsushima Strait SCM (TS_SCM), East China Sea surface (ECS_S) and East China Sea SCM (ECS_SCM).

BGD
10, 14475–14514, 2013

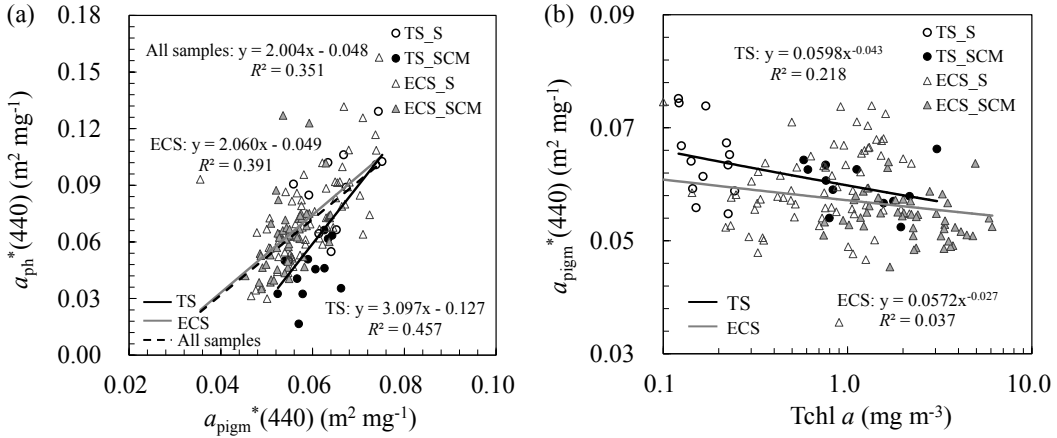

Fig. 8. Variations of $a^*_{pigm}(440)$ vs. $a^*_{ph}(440)$ **(a)** and Tchl *a* **(b)** in the Tsushima Strait surface (TS_S), Tsushima Strait SCM (TS_SCM), East China Sea surface (ECS_S), and East China Sea SCM (ECS_SCM). Black and grey solid lines indicate linear regressions in the Tsushima Strait (TS) and East China Sea (ECS), respectively. Black dashed line is the linear regression for all samples.

BGD
10, 14475–14514, 2013

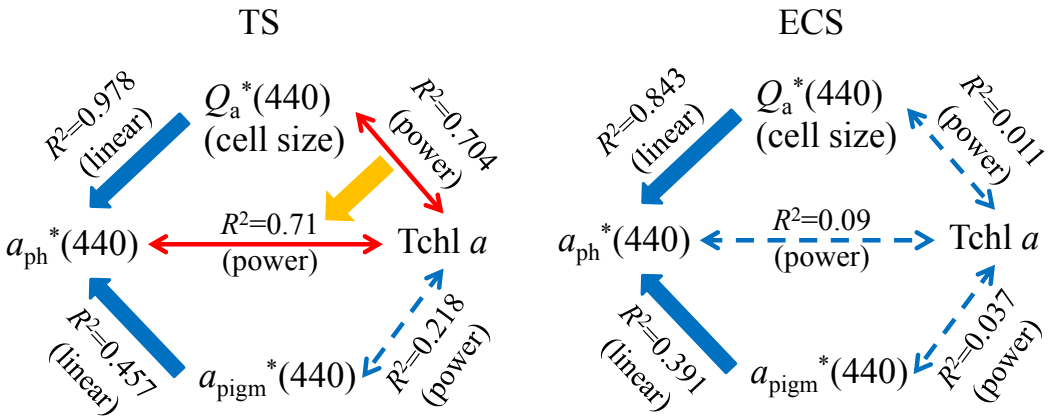

Fig. 9. Summary of the relationships among $a^*_{ph}(440)$, $Q^*_a(440)$, $a^*_{pigm}(440)$, and Tchl *a* in the Tsushima Strait (TS) and East China Sea (ECS).

BGD
10, 14475–14514, 2013